Journal of Magnetism and Magnetic Materials 485 (2019) 391–400

Contents lists available at ScienceDirect

Journal of Magnetism and Magnetic Materials

journal homepage: www.elsevier.com/locate/jmmm

Research articles

Repeatability and stability study of residual magnetic field for domain wall characterization

Kun Zeng[a], Guiyun Tian[a,b,*], Jia Liu[a], Bin Gao[a], Fasheng Qiu[a]

[a] School of Automation Engineering, University of Electronic Science and Technology of China, Chengdu, Sichuan 611731, China
[b] School of Engineering, Newcastle University, Newcastle upon Tyne NE1 7RU, United Kingdom

ARTICLE INFO

Keywords:
Residual magnetic field
Stress characterization
Repeatability and stability
Magnetic domain motion

ABSTRACT

Residual magnetic field (RMF) for metal material has a relationship with material stress status. Bridging the relationship between macro parameters and material microstructure is an essential step to deal with the characterization of residual stress. This paper applies magneto-optical Kerr microscopy (MOKE) with the help of magneto-optical indicator film (MOIF) to observe and analyze variations of magnetic domain pattern under different stress conditions of high permeability grain oriented electrical steel (HGO steel). Experiment about repeatability is carried under cyclic stress applications and the stability study is proceeded during the relaxation time after release of stress. By using two domain texture features, mean value (MV) of domain wall image intensity linked to domain rotation to characterize RMF amplitude and the angular second moment (ASM) related with domain wall displacement to express the RMF distribution are used for investigation of repeatability and stability. Results show that domain wall displacement is repeatable and stable both under cyclic stress round and during relaxation time after release of stress. It has been found that the situation of domain rotation is varied in different locations, and broad texture area of domain wall images has better repeatability and stability when compared with area with narrow texture of domain wall images. The results provide substantial potential to evaluate the residual stress from the view of characterization of micro-structure.

1. Introduction

Most engineering materials in service work under stress and RMF receives significant interest from the demand of early damage detection and stress concentration [1-3]. Wilson [4] found that RMF variation and pattern can be used for assessing stress and its detection, also the applied stress has a closer relationship with the parallel field component. Roskosz used the pattern of isoclines to study the distribution of RMF signal, and a good relationship between the value and the distribution of the gradients of RMF and residual stress were put forward in his follow-up study [5,6]. In addition, the amplitude and frequency of load, the shape of sample, the testing direction and lift-off value were analyzed [7–10]. In the meantime, theoretical investigations about RMF were undertaken. Xu used Jiles-Atherton model (J-A model) to clarify the Metal Magnetic Memory (MMM) in the elastic stage [11]. Shi presented an analytical magnetic charge model to simulate 3D MMM signal [12,19]. Li used permanent installed magnetic sensors array to study how the stress history affects the MMM signal [20].

However, those studies mainly focus on the macroscopical view to study RMF, whereas there are few papers presenting their link to microstructure. Since most magnetic materials are polycrystalline consisting of crystal lattices of separate grains oriented in random directions, each grain has an easy axis of magnetization and is divided into domains with the axis of magnetization and parallel to this axis in alternate direction, making it practically valuable to discuss the RMF distribution in different locations in a sample. In this paper, a HGO sample is used for the study because of its excellent electromagnetic properties, and the large magnetic domain size makes the microstructure characteristics much easier to be observed.

Compared with Transmission Electron Microscope, Magnetic Force Microscope, Atomic Force Microscope and many other microscopic imaging techniques, Magneto-optical (MO) method based on rotation of polarization of light reflected from a magnetized surface is able to observe dynamic domain structures and to determine the magnetic characteristics of material in a cheaper and more convenient way [11–15]. In this paper, magnetic domain microstructure captured through MO method by MOKE is used to characterize the RMF. Two statistics features are presented to characterize the RMF signal. The normalized mean value (MV) feature demonstrates the amplitude of RMF signal through calculating the mean value of domain image intensity, which is

* Corresponding author at: School of Automation Engineering, University of Electronic Science and Technology of China, Chengdu, Sichuan 611731, China.
E-mail address: g.y.tian@ncl.ac.uk (G. Tian).

https://doi.org/10.1016/j.jmmm.2019.04.082
Received 9 December 2018; Received in revised form 30 March 2019; Accepted 24 April 2019
Available online 25 April 2019
0304-8853/

regarded as a scope of domain rotation. The angular second moment (ASM) feature expresses the distribution of RMF signal by computing the domain texture sparsity, and this feature is related to domain wall displacement [22]. We focus on the repeatability and stability of RMF signal and highlight the difference of feature behavior affected by regional effect. More importantly, this macro magnetic property is discussed from point of view of microstructure, which is useful to reveal the origin of microstructural behaviors in MMM method.

The paper is organized as follows: after the introduction, Section 2 introduces the methodology of experiment. Section 3 shows the sample preparation and Section 4 reports the results and analysis. Conclusion and future work are summarized in Section 5.

2. Methodology

The MOKE observation system with help of MOIF is used to capture magnetic domain image in this paper. After image acquisition, RMF characterization through magnetic domain is put forward and the bridge of correlation is established (between?). To study the repeatability and stability, experiments about cyclic load-and-unload stress application and domain behavior after release of stress during the relaxation time are presented.

2.1. Experimental system

The MOKE microscopy system is used to observe magnetic domain behavior together with the calculation of macroscopic magnetic properties, such as coercive, remanence and hysteresis loss. The physical mechanism of MOKE is that the intense internal magnetic field of sample causes a rotation of the polarization plane of the polarized light either in reflection from an opaque material. The sensing and magnitude of rotation depend on the direction and density of domain magnetization. Therefore, domain magnetization in different directions impart different rotations to the reflected or transmitted light, and the domain structure is visible in light-dark contrast when the sample is viewed through an analyzing prism set to extinguish one of the rotation.

The MOKE microscopy is based on the magneto-optical Kerr effect. However, a convenient and faster way to visualize the magnetic domain appears, it's domain imaging by MOKE with the help of MOIF, where higher contrast and more details can be provided by the domain images without sample surface polish. The schematic diagram of MOKE and MOIF is shown in Fig. 1.

The MOIF was first used in the study of superconductors and widespread used in material science and magnetic microstructure distribution [15,16]. The transmission analogue of Kerr effect and the Faraday effect finds an important application in MOIF to map stray field above the investigated specimen, even the unpolished sample. The MOIF is composed of a thin mirror layer, a transparent substrate and a magnetic garnet layer. Polarized light enters the MOIF, which is placed on the top of magnetic sample, passes through the substrate and the magnetic garnet layer, then is reflected by the mirror and passes the garnet layer again, this is the process by which a Faraday rotation is induced.

2.2. Characterization of RMF using domain texture

The Faraday rotation depends on the magnetic field normal component B, the frequency-dependent Verdet constant V, and the traversed length l of MOIF, which equals to the distance light runs in the substrate and garnet layer [17]. The Faraday rotation angle α can be described as:

$$\alpha = BlV \tag{1}$$

According to the Malus law [18], when a beam of light passes through a light path which consists of an ideal polarizer and analyzer, the light intensity I is given by

$$I = I_0 cos^2\,\theta \tag{2}$$

where the I_0 is the initial intensity and θ is the angle between polarizer and analyzer. In this paper, the real light path will be rotated by the Kerr and Faraday effect, making Eq. (2) change into

$$I = I_0 cos^2(\theta + \alpha + \beta) \tag{3}$$

β stands for the Kerr rotation which is relatively small and the value is less than 1°, and in this experiment, θ is set to 120°, to make it simplify, $\theta + \beta \approx 120$Â°.

To express the difference between the initial and measured signal, the MOKE and MOIF signal is

$$\begin{aligned} I= &\ I_0 cos^2(\theta + \alpha + \beta) - I_0 + I_0 \\ = &\ I_0 - I_0 sin^2(\theta + \alpha + \beta) \\ = &\ I_0 - I_0 sin^2(\alpha + 120°) \end{aligned} \tag{4}$$

Expanded by Taylor series and only regard the first two items, Eq. (4) is achieved as

$$I = I_0\left[\frac{\sqrt{3}}{2}(120Â° - \alpha) + \frac{3}{4}\right] \tag{5}$$

Merging the Eqs. (1) and (5), a new equation about I is

$$I = I_0\left[\frac{\sqrt{3}}{2}(120Â° - BlV) + \frac{3}{4}\right] \tag{6}$$

Thus the relationship between normal component of underlying magnetic field B and the intensity of the magnetic domain image I can be given as

$$B = \frac{120Â° - \left(\frac{\Delta I}{I_0} + \frac{1}{4}\right)\frac{2\sqrt{3}}{3}}{lV} = \frac{120Â°}{lV} + \frac{\sqrt{3}}{2lV} - \frac{2\sqrt{3}}{3lVI_0}I \tag{7}$$

In the experiment in this paper, l and V are invariant parameters, the Eq. (7) can be summarized as $B \propto I$, thus the magnetic field can be characterized by the domain image intensity.

The MOIF itself doesn't generate stray field, but it can reflect the stray fields emerging from the underlying magnetic sample, thus causing a Faraday-contrast pattern that depends on the microstructure pattern in the specimen. The MOIF technique is considered as an indirectly imaging method to visualize the stray field distribution above the sample surface in the sensor plane, and hence gives a deep insight into the magnetic domain configuration in the sample. As the image of magnetic domain and the relationship with microstructure in HGO sample shown in Fig. 2, the stray field is generated by two potential sources, one is domain magnetization and the other is domain wall. The different stray fields thus leading to different gray value (intensity) amplitude and texture distribution in MO image and the MO image represents the underlying RMF signal in return. In this paper, two features are used to characterize the RMF signal both in amplitude and distribution [22]. The normalized mean value of intensity is:

$$MV = \frac{\sum_{i=1}^{m}\sum_{j=1}^{n} I(i,j)}{MV_{max}} \tag{8}$$

where i and j are coordinates of the corresponding pixel points. It is defined as the average value of domain image intensity normalized by the max average domain intensity value in a corresponding area to remove the influence of the experiment environment on the test results. As the intensity is the reflection of the amplitude in one single point, the mean value is a sign of the RMF signal amplitude. Domain rotation (DR) and domain wall displacement (DWD) are the two major domain motions, and those motions cause variations in the MO image and MV feature. In the microstructure, the thickness of domain wall (σ_{DW} ~60 nm) is much smaller than domain width D, and it has less effect on the change in the MV feature. In this way, the DR is the main driver of MV changes for rotation in single point which causes large domain

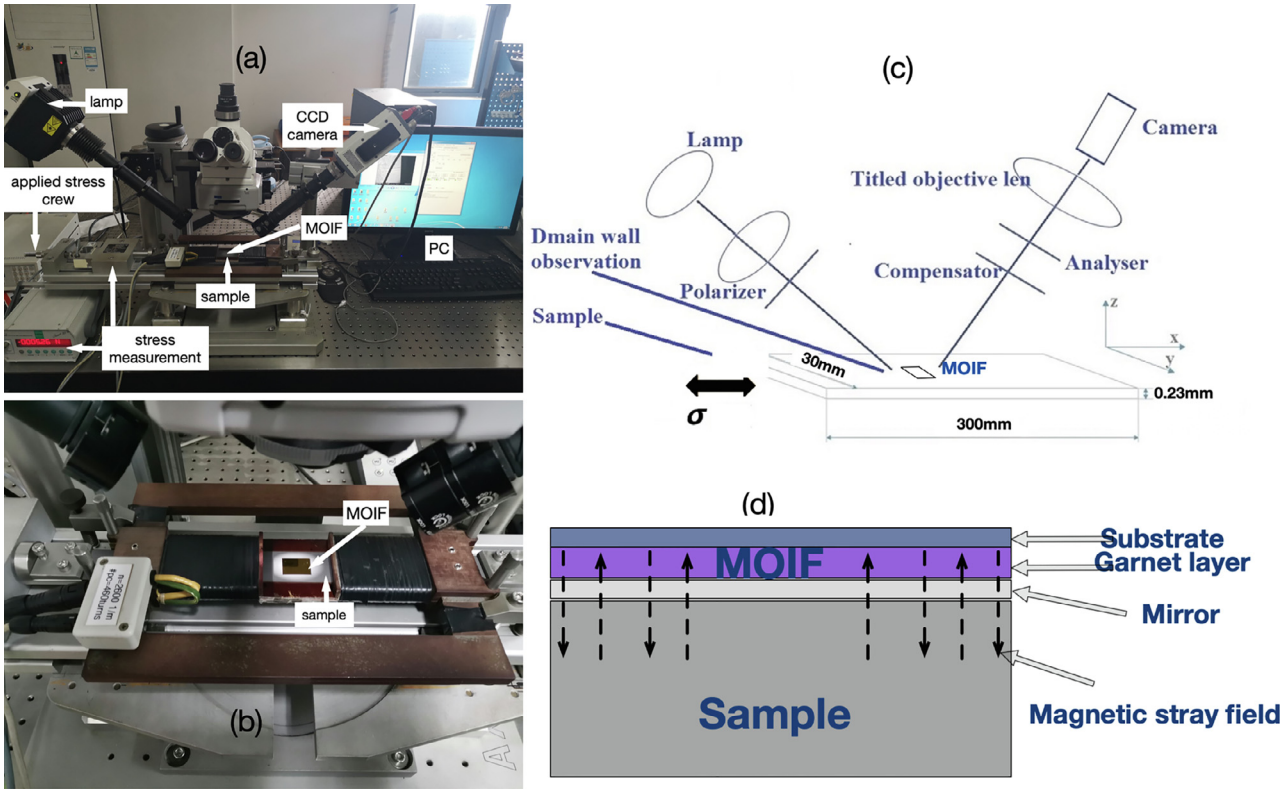

Fig. 1. The schematic diagram of MOKE and MOIF. (a) photo of MOKE observation system; (b) placement of MOIF; (c) schematic diagram of the MOKE set-up; (d) basic principle of the domain pattern measurement by using the MOIF.

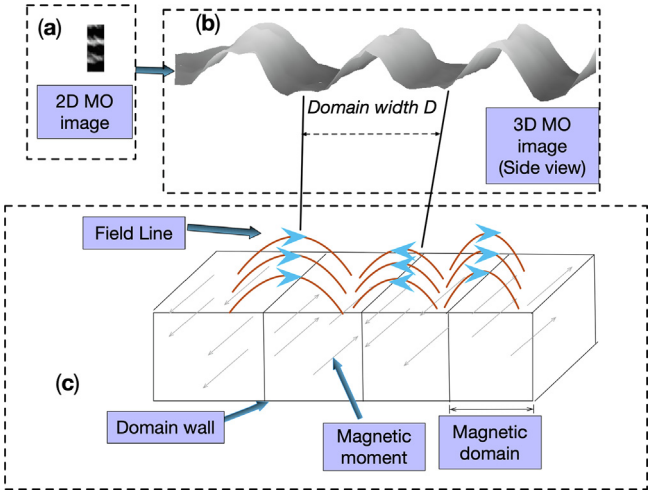

Fig. 2. MOKE image and the relationship with magnetic microstructure. (a) is the 2D MO images (size: 1 mm*3 mm). The 3D side view of (a) is shown in (b), and (c) is the corresponding model of domain and domain wall structure in the sample.

image intensity vibration.

Even if the MVs are the same, a variety of texture forms exist in the MO image, making it hard to directly distinguish and quantify the differences in local areas. In this work, a second-order statistics feature, normalized angular second moment, also called as texture energy, which based on gray level co-occurrence matrix (GLCM) is provided as:

$$ASM = \frac{\sum_{i=1}^{m}\sum_{j=1}^{n} I(i,j)^2}{ASM_{max}} \quad (9)$$

where i and j are coordinates of the corresponding pixel points. ASM presents the uniformity of the captured images, and it is the measurement of the stability degree of the gray change of the texture, which reflects the uniformity of the gray distribution and the degree of texture. As a texture pattern assessment criteria, ASM is mainly affected by the DWD and it's an evaluation means to illustrate the characterized RMF distribution. By using MV and ASM, both the magnitude and distribution of RMF can be characterized and identified by domain texture.

2.3. Diagram of the approach of the experiment

The system diagrams of domain capture, RMF characterization and experiment procedure are shown in Fig. 3.

Fig. 3(a) shows the whole steps to do observation and analysis of domain wall in repeatability and stability experiment. The first stage includes experiment and sample preparation. Then in the repeatability experiment in Fig. 3(b), the sample was firstly loaded to a pre-set tensile stress (PSS), and kept for 0.1 min, then the stress application is removed and the sample is placed on the platform without any treatment, the domain pattern image is captured by the CCD camera of MOKE. After the image acquisition, the above procedure is repeated with another PSS. In each round, the PSS is increased with a 14.5 MPa stress interval and finally until the sample is loaded to 87 MPa stress application, one round of loading is formed. To see the how historical loading affects the domain pattern, totally 8 loading rounds are induced but the time intervals between each round are not the same. The detailed time intervals between two adjacent rounds are listed in Table 1.

Another experiment to discuss the stability of characterized RMF signal is conducted as Fig. 3(c). Firstly, the 29 MPa PSS is applied to the sample and removed 0.1 min later, then the sample is left in a relaxation state and domain images are recorded by CCD camera during the next 1440 min. After the image acquisition, three similar experiments are carried again, but another two PSS are 58 MPa and 87 MPa, respectively.

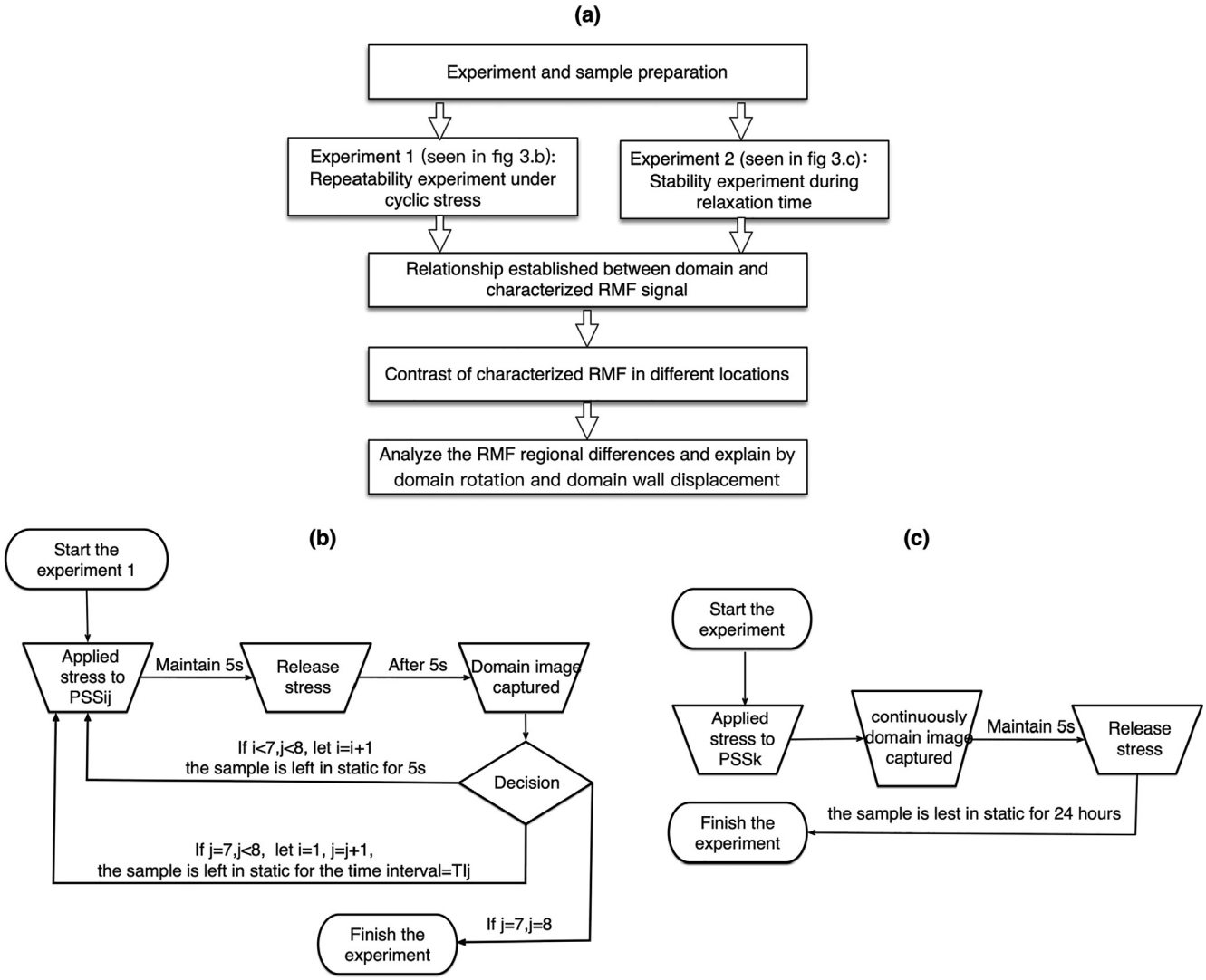

Fig. 3. Systematic diagrams of the investigation (a) procedure of domain observation, correlation between DW and RMF establishment and result analysis; the detail experiment progress of (b) the repeatability study, Where the i and j stand for the i-th pre-set stress application in the j-th round respectively, and the PSS_{ij} is the pre-set tensile stress; (c) the stability study, Where the k stands for the k-th pre-set stress application.

Table 1
The detailed time interval TI_{ij} between i-th and j-th rounds.

TI_{12}	TI_{23}	TI_{34}	TI_{45}	TI_{56}	TI_{67}	TI_{78}
0.1 min	1 min	30 min	60 min	240 min	720 min	1440 min

After the experiment, basic relationship of RMF and stress application is established, the amplitude and distribution of RMF signal under cyclic stress application and during relaxation time are demonstrated. Through dividing the sample into three different local areas with different domain pattern, the location differences are discussed. Finally, domain rotation and domain wall displacement are used to explain the reginal difference.

3. Sample preparation

In this study, a HGO electrical steel sheet sample which holds a ⟨0 0 1⟩ Goss texture along the rolling direction is employed. The sample with the shape of 0.23 mm thickness, 30 mm width and 300 mm length is typed 23Z110. In this paper, all the tensile stress is applied parallel to the rolling direction. The yield stress of the sample is 300 MPa and all the stress relevant applications in this paper are discussed within the range of elastic strain. With an insulation coating applied on the surface, unless it goes on a polishing treatment, MOKE can only observe it with the help of MOIF. Without any treatment, the initial domain pattern of overall measured area is shown in Fig. 4(a). To highlight the local difference, three typical local areas with different size of domain are chosen and the distribution is shown in Fig. 4(b–d).

To exclude the external environment influence, the experimental state was kept in a constant state of 24° temperature, 40% humidity, incident light of 275 lm and away from external magnetic field.

4. Results and discussions

In the load-and-unload progress, domain varies with stress, both in single point and distribution (seen in Fig. 5a–d). Domain patterns are different when the stress is applied or removed, and to illustrate the difference directly, the relationship between texture features and applied stress of the overall area in the first loading round is shown in Fig. 5(e) and (f). Features become larger while stress application increases, but they vary under different stress statues. Generally, when applied with stress, the contrast of domain image increases together with the texture becoming narrow. After release of stress, the domain immediately reverts to its original state, but the residual stress causes

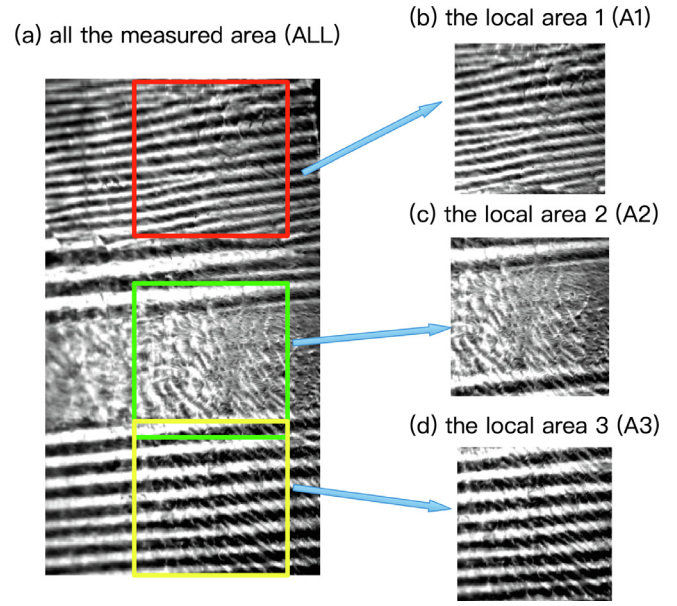

Fig. 4. The whole measured area (size: 18 mm*10 mm) and the distribution of three difference local areas (size 6 mm*6 mm).

pinning and lattice defect block this process, making the amplitude and distribution of RMF both can't return to what they were initially. Besides, the changing tendency and the feature values also indicate that the DR and DWD responses to stress are not synchronous. The larger fluctuation in MV features, especially in the unload state, making it not stable enough when compared with ASM feature.

The domain patterns vary significantly in different local areas, to demonstrate the regional disparity and make a directly comparison with the overall area, the features at different local areas and their relationship with different stress statues are shown in Fig. 6. It's worth mentioning that in the lower stress level, domain in the middle of local area 2 is sightless, but when the stress application is increased to a higher level, it's become visible.

Features in all the local areas behave similarly with overall area, but the MV shows a complex and changeable performance in different areas both with stress application and after release of stress. Domain width *D* in local area 1 is the narrowest, and it reached the peak MV value when the stress application is 43.5 MPa both when stress is applied or removed. Stress beyond 43.5 MPa causes minor effect on the DR motion, leaving the amplitude of characterized RMF signal change in a small scale during this stress level. The opposite change trend appears in local area 2, where the domain width *D* is complex under different stress statues. In the low stress level, a large width domain exists in the middle of this area, but as the applied stress increases, this large width domain is divided into several small width domains, and further increase of stress makes those newly emerged domains become narrower. This abnormal behavior makes MV value quickly reach a temporarily stable state at the stress state of 14.5 MPa, subsequently, in the low stress range, domain doesn't change significantly when higher stress is applied. Thereafter, stresses exceeding 43.5 MPa cause the domain continue to rotation, and the MV feature rapidly rise linearly to the maximum. The MV feature of local area 3 behaves a linear relationship with loading stress, and when the stress application is larger than 43.5 MPa, the MV feature of local area 3 is very close to the MV feature of local area 2, and in this stress range, the domain width *D* in the two local areas are similar. Besides, after the release of stress, local area 3 holds the largest MV feature, meaning that 33.5% of stress induced DR in local area 3 is irreversible after the stress is removed. The percentage is 12.2% of local area 1 and 21.2% of local area 2. As an average of all local areas, the overall holds a 24.8% percentage of remained DR.

The ASM feature is more stable with stress change in Fig. 6(b). Both in loading state and unload state, the linear relationship between stress and ASM is approximately steady and the DWD motion is more disciplined to the stress change. The distribution of RMF signal is the similar sort as the amplitude of RMF signal, and eventually, the ASM in overall is the median of all the areas.

As a summary, both the amplitude and distribution of characterized RMF signal are highly affected by the local area effect, and in general, domain with narrow domain width *D* is more sensitive to stress but the DR and DWD are easier to return to the initial state, the domain with broad domain width *D* is on the contrary. In another hand, the characterized RMF has a relatively stable distribution which is stick to the former stress application. The amplitude of characterized RMF is also a method to evaluate the former applied stress, but vibration of this feature makes it not stable enough.

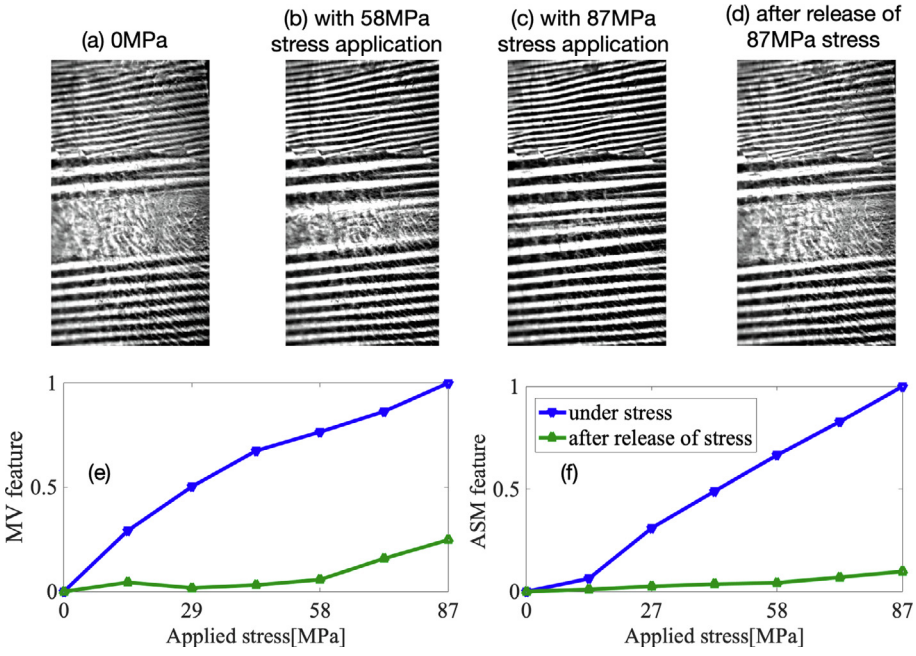

Fig. 5. Relationship between features and stress of the overall area in the first round and the related domain images. (a) is the domain image before the experiment without any stress application; (b) and (c) are domain images captured then the sample is applied with 58 MPa and 87 MPa tensile stress; (d) is the domain image captured 5 s after the release of 87 MPa tensile stress application; (e) shows the relationship between MV and stress statues in the whole measured areas and (f) is the similar correlation between ASM and stress statues.

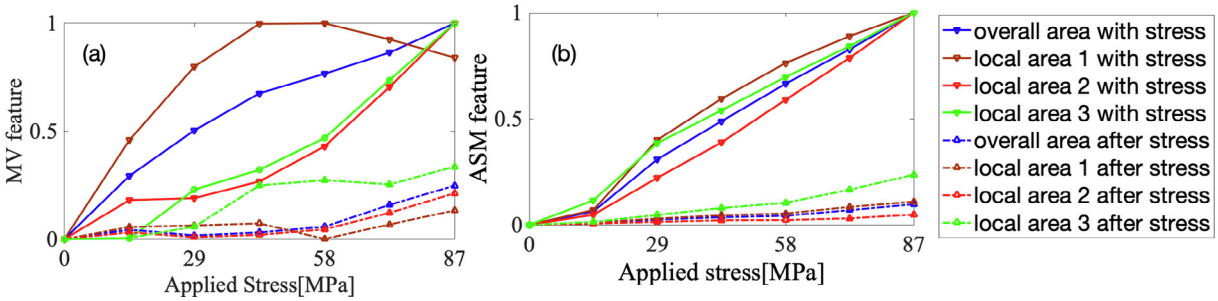

Fig. 6. Texture feature at different areas in the first round.

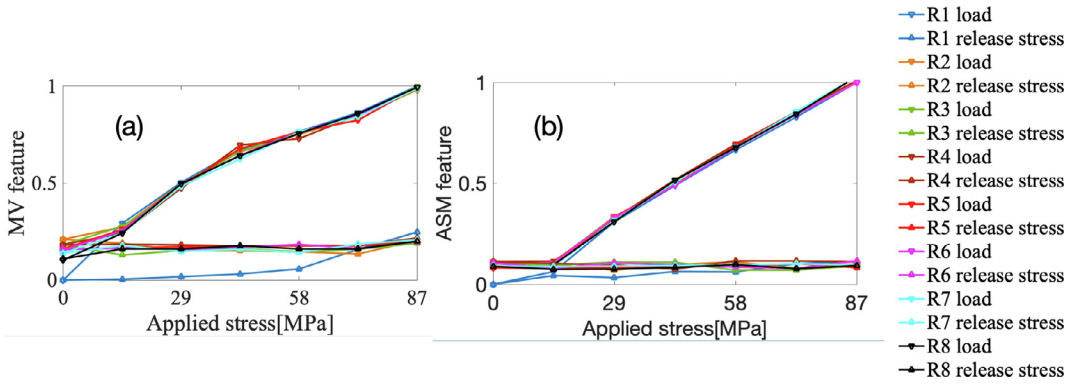

Fig. 7. (a) MV and (b) ASM feature in overall area about repeatability in different cyclic stress rounds.

4.1. Repeatability in cyclic stress applications

Features of characterized RMF signal under seven rounds of cyclic stress applications and after the release of stress are discussed in this section.

Curves of MV feature and ASM feature under cyclic stress application are shown in the Fig. 7. Two types of feature-stress relationship curve are shown in this figure, one is the features when applied with stress and the other is the features after release of stress. The first round is much different from next seven rounds, especially the MV feature and ASM feature after release of stress in this round. Before the start of experiment, the sample is in a stress-free state but the stress application disturbs it. DR and DWD is induced by the applied stress but not all the components revert to initial state after release of stress. In the start of round 2, the MV and ASM feature aren't equal to zero, and both of them have residual components of DR and DWD. When the stresses are applied, the DR and DWD change obviously. But when the stress is removed, the residual components caused by the maximum previously applied stress (87 MPa) changes little, so in the Round 2 to Round 8, all the two features stay on oscillatory equilibrium state. The residual components fade with time, and as the time interval between two adjacent rounds increases, the MV feature values at zero applied stress in each round go down. In the same time, the start ASM feature values at zero applied stress in each round are almost the same. This variation indicates the residual components of stress induced domain motion will continue to change towards the initial state with the increase of time, and the change of DR and DWD isn't synchronous, the DR towards the zero-stress state is continuous while the DWD is relatively weak.

To take a further study of regional difference, repeatability of MV feature and ASM feature in local areas is taken into consideration. Fig. 8 shows the MV feature in three local areas under stress applications and after release of stress. It's much similar to the overall situation in the Fig. 7 when under stress. In Fig. 8(a), (b) and (c), except the 0 MPa state, no matter in which round, the MV feature values are almost equal when applied with a same stress. This result indicates the level of domain rotation are approximately the same whenever a same stress is applied. But in the zero stress state, MV features vary in different local areas. No stress was applied before the first round, so MV features in three local areas are all zero at 0 MPa state. But in the next seven rounds, the 0 MPa state is actually the relaxation state caused by the 87 MPa stress application in last round. The DR caused by last 87 MPa reverts towards the initial no stress state after release of stress, and this reversion isn't a transient process. The MV feature of 0 MPa is roughly in a declining state as the time interval increases, thus the recovery speed of DR in different local areas are inconsistent, making the MV features at 0 MPa state are different. The detailed feature stability behavior during relaxation time will be detail discussed in next section.

The focus moves to the state after release of stress, as mentioned above, the features in the stress-free state are the points. The results of MV feature after release of stress in different local areas are demonstrated in Fig. 8(d–f). Except the phenomenon that the MV features are affected by the time interval at the 0 MPa state, another point is that even after release of a same stress, the MV feature is vibration. The most intense feature float exists in the local area 1 and the minimum value is 25.0% of the maximum value in a same stress (after 87 MPa), and the ratio are 52.0% and 69.0% in local area 2 (14.5 MPa) and local area 3 (43.5 MPa).

As a contrast, the ASM feature in the three local areas under stress applications and after release of stress is shown in Fig. 9. The feature appears similar with MV feature in Fig. 8, but the magnitude of fluctuation is different. Table 2 shows the comparative result of repeatability under cyclic stress (after release of stress) in different areas. According to the standard deviation (SD) result, when in a same local area, the SD of MV feature is several times larger than it of the ASM feature. As a result, the DWD isn't as violent as DR, and it's much repeatable under cyclic stress applications. The comparisons of SD in local areas also provide information about regional variation in repeatability. The SDs of the two features in local area 1are the largest and the domain width D is the narrowest. On contrary, the SDs of the two features in the local area 3 where the domain width is the broadest are the smallest on the whole. The local area 2 locates at the conjunction of the above two local areas, and the domain in this area is

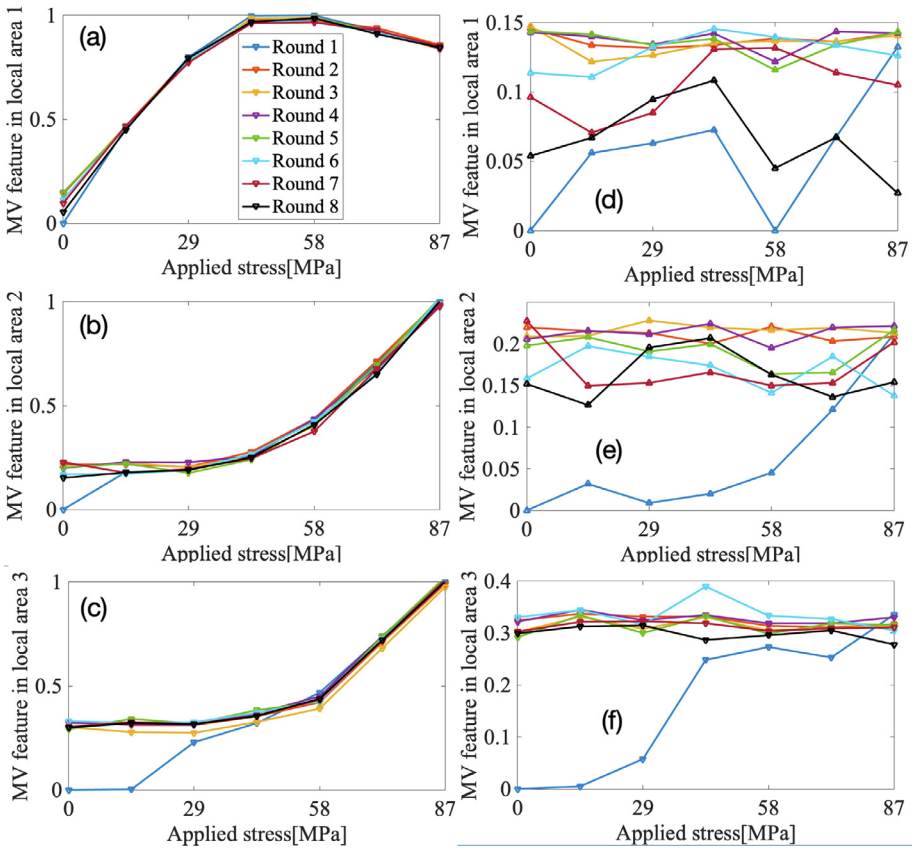

Fig. 8. MV feature in local areas about repeatability in different cyclic stress rounds. (a)–(c) is MV under stress in the local areas 1, 2 and 3; (d)–(f) is MV after release of stress in the local areas 1, 2 and 3.

partly similar to the domain in local area 1 and partly similar to the domain in local area 3.

4.2. Stability during relaxation time after release of stress

The MMM signal is not a stable method and it degrades with time delay, and many researchers found abnormal phenomenon in their studies [5,21]. This variability originates from the domain dynamic, and the DR and DWD are the main sources.

The repeatability result shown in Section 4.1 shows that the ASM feature is relatively repeatable in cyclic stress rounds with different time interval, and the stability result confirms it. Because the results in different areas are much similar, only the result of ASM during relaxation time in the whole measured area is discussed as shown in Fig. 10. After release of stress application, the ASM feature quickly recovers to the relatively stable residual value, and the stress induced DWD quickly revert towards its initial state but the irreversible component and some part of the reversible components are still suffering from residual stress. During the next 1440 min, the ASM continue to resist a tiny fluctuation tendency. In this phase, DWD is continuous, but isn't as dramatic as the period when the stress is just removed. Different pre-load stress has a similar consequence in the relaxation time, and the DWD is steady within 5% of ASM feature float.

As a contrast to ASM, the MV feature is totally different. Fig. 11 shows the MV feature in local area 1, 2 and 3, respectively, during the relaxation time after release of different stress applications. Fig. 11(a), (d) and (h) are the panorama of the MV feature variation during the whole 1440 min relaxation time. To have a further look into the detailed information, the relaxation time is divided into two parts. The first part starts from the moment the stress is removed and lasts 5 s, this period is called as B TIME and the results are shown in Fig. 11(b), (e) and (h). The MV feature in this period quickly decreases once the stress is removed. In the B TIME, MV feature after release of stress quickly decreases to a relatively stable value, and in different locations and after different stress, the stable value is not the same. The regional difference also exhibits in the time required to reach the relatively stable value. In the local area 1, the time is about 3.5 s, in the local area 3, this time is 5 s, and in the local area 2, 4.2 s is needed to reach the state. The local area 1 with the finest domain need the least time to drop rapidly. The second part (seen in Fig. 11(c), (f) and (i)) is a long-term relaxation process, and is called as C TIME. In the C TIME, the MV feature continues to decrease but much less violent as the first part. After quickly falling to a value of about 0.16, MV feature continues to and in the next 1440 min' relaxation time, the MV feature value in local area 1 decrease from 0.16 to 0.06 and then vibrates in the next time in the range 0.04 to 0.08. The broad domain in local area 3 leaves it costs the most time on reaching to the stable value, and in the relaxation time, the slight decrease is on-going. The range of the MV feature value in the local area 3 is 0.27 to 0.35. In the middle of those two areas, MV feature in the local area 2 has similarities with both of the areas. The feature in B TIME is similar with local area 1 but in the C TIME is more like the area 3.

The two periods in the relaxation time can be explained by the flake-like magnetic domain and lancet in them. Once the stress is released, the big flake-like domain has the ability to quickly move and release the residual stress, so in the B TIME the MV feature descends quickly. After the recovery of flake domain, the lancet in them are still affected by the surrounding flake domain conjunction with residual stress. In the C TIME, slightly residual stress variation occurs and it just makes little influence on the flake domain rotation. Thus the feature in this period stays at relatively stable statue, but the magnetization of the flake domain blocks the domain motion of inner small lancet, causing them to keep moving, and this sustained movement finally is reflected in the MV feature fluctuation.

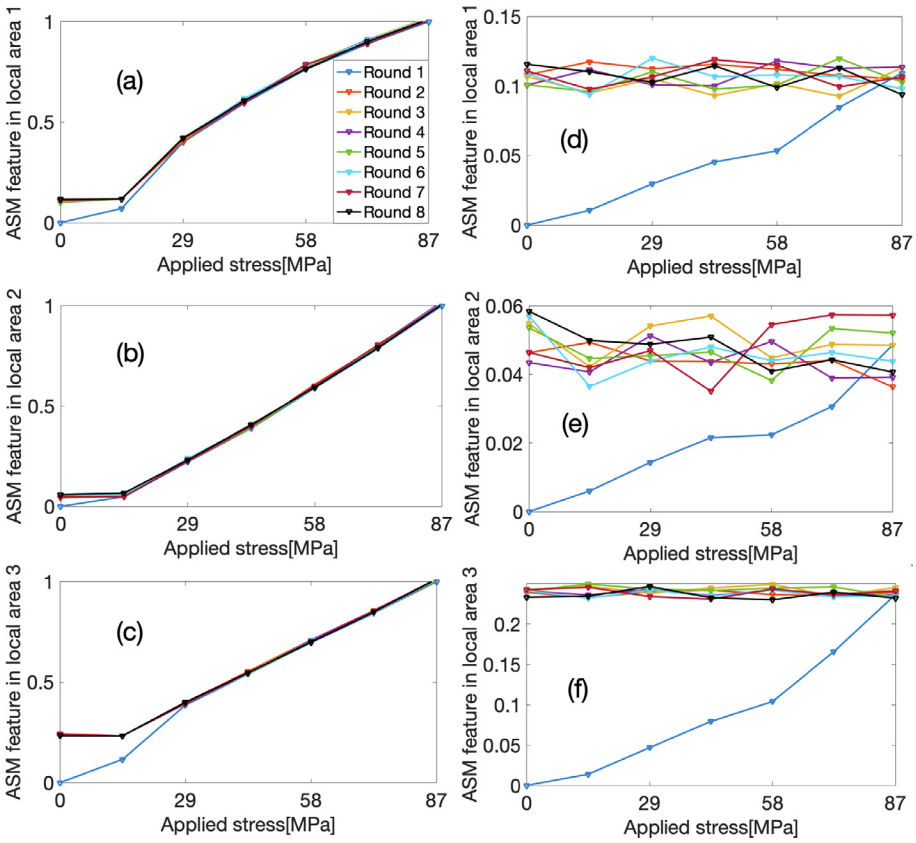

Fig. 9. ASM feature in local areas about repeatability in different cyclic stress rounds. (a)–(c) is ASM under stress in the local areas 1, 2 and 3; (d)–(f) is MV after release of stress in the local areas 1, 2 and 3.

5. Conclusion and future work

This paper investigates the RMF characterization by using domain wall texture observation. Magnetic domain in this paper is captured by the MOKE microscopy system with the help of MOIF. In order to bridge the relationship between microstructure and macro-characteristics, domain texture features are used. The magnitude of RMF is characterized by MV of the domain image intensity and the distribution is expressed by the ASM. Experiments of repeatability under cyclic stress and stability during relaxation time after release of stress are carried out. Results show that DWD is repeatable in cyclic stress rounds and stable during the relaxation time after release of stress. Some points of differences in the domain rotation below have been found:

1) When applied with a same stress, the domain rotation (DR) is approximately the same depending on the repetitive applied stress rounds. The more rounds of stress applied, the less difference of domain rotation. The time interval between two adjacent rounds only makes influence on the zero-stress statue of next rounds, and initial value is based on the time interval. With a longer time interval, the domain is likely to rotate to the zero-stress statue.
2) After release of same stress, the residual states of DR are inconsistent. In the area with narrow domain texture, the minimum value is about 25.0% of the maximum value in a same stress, but in the area with broad domain texture, the ratio is much higher and is about 69.0% when after release of same stress. The repeatability of DR under cyclic stress is highly influenced by the domain width, the domain with broadest width is about 2 times more repeatable than the domain with narrowest width.
3) During the relaxation time, the DR process can be divided into two stages. The former one is the rapidly decrease stage (B TIME), and during this time, domain quickly rotates towards the initial state. But the residual stress blocks the motion, preventing the domain from reaching the no stress state. After the B TIME, domain continues to move during the next time (C TIME), because the domain is now affected by the lattice and the geomagnetic field, the change trend here is fluctuating.
4) During the B time, in the area with narrow texture, domain rotation towards initial state is faster than in the area with sparser texture. During the C TIME, domain continues to move towards the initial state, but in the narrow texture area, the descending percentage is 62.0% while in the broad texture area, this percentage is only

Table 2
Comparative result of repeatability under cyclic stress (after release of stress) in different areas.

Area	Standard Deviation	0 MPa	14.5 MPa	29 MPa	43.5MPa	58MPa	72.5 MPa	87 MPa
Local area 1	MV	0.0353	0.0315	0.0208	0.0122	0.0336	0.0265	0.0426
	ASM	0.0053	0.0077	0.0307	0.0100	0.0075	0.0091	0.0073
Local area 2	MV	0.0195	0.0259	0.0144	0.0128	0.0221	0.0228	0.0234
	ASM	0.0059	0.0041	0.0131	0.0058	0.0055	0.0062	0.0057
Local area 3	MV	0.0148	0.0117	0.0106	0.0304	0.0131	0.0076	0.0162
	ASM	0.0033	0.0071	0.0310	0.0053	0.0061	0.0042	0.0046

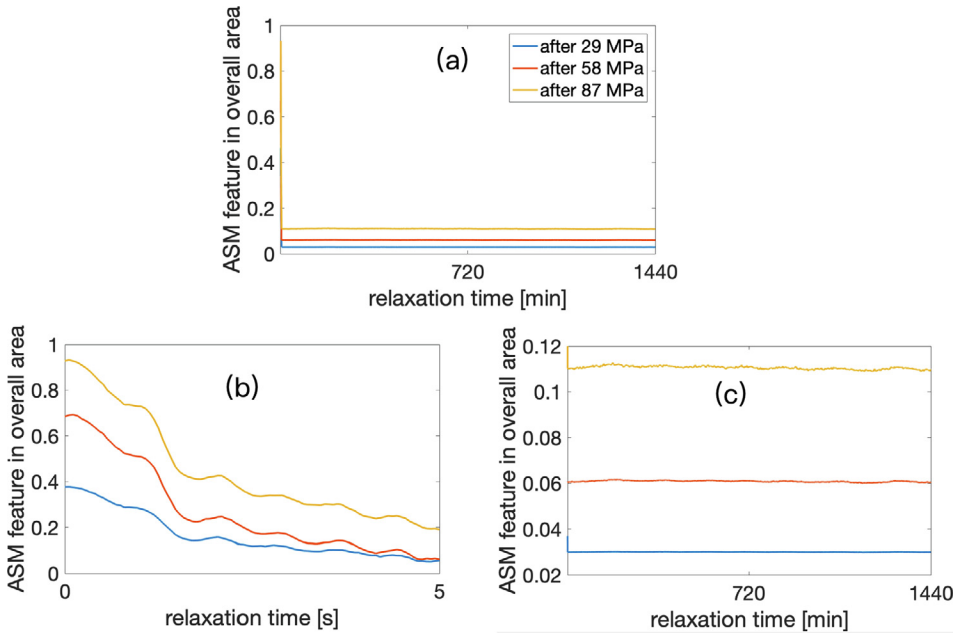

Fig. 10. ASM during relaxation time in the overall area. (a) is the feature change during the whole 1440 min after release of stress; (b) is the detail variation in the first 5 s and (c) is the changing situation during 5 s to 1440 min.

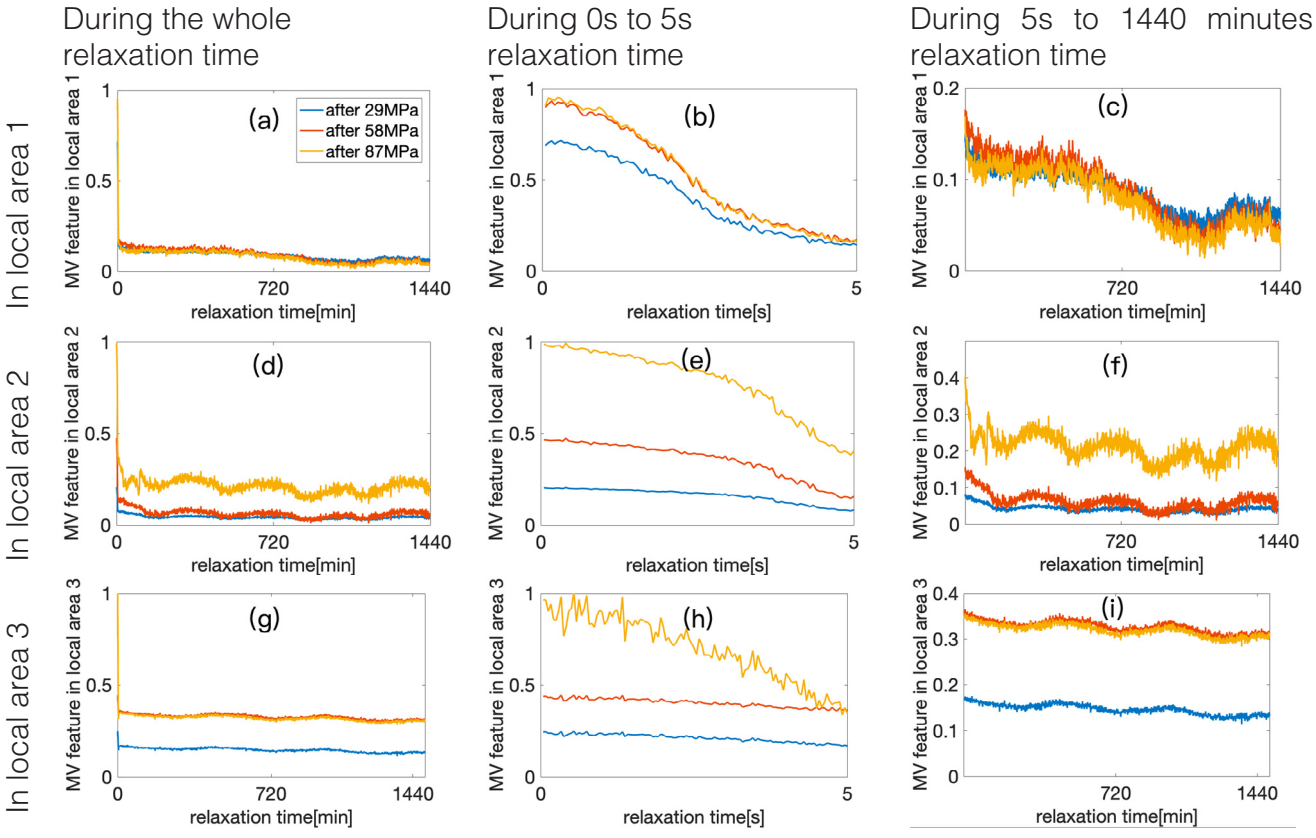

Fig. 11. MV feature during relaxation time after release of different stress application in local areas. (a) in the 1440 min hour relaxation time in local area 1;(b) the detail change in the beginning 5 s after release of stress in local area 1; (c) change from 5 s to 1440 min in the local area 1; (d) in the 1440 min relaxation time in the local area 2; (e) the detail change in the beginning 5 s after release of stress in local area 2; (f) change from 5 s to 1440 min in the local area 2; (g) in the 1440 min relaxation time in the local area 3; (h) the detail change in the beginning 5 s after release of stress in the local area 3; (i) change from 5 s to 1440 min in the local area 3;

18.0%. The situation in the junction of those two areas shows a transitional trend.

The repeatability and stability of domain motion in the broad microstructure area is much better than narrow domain area. In the future, different samples will be used to study the behaviors of regional differences in grains and at the grain boundary, also the grain size and mis-orientation will be taken into consideration. In addition, modified J-A model will be included in the calculation of domain motion to make a further step to analyze and establish the micro and macro relationship.

Acknowledgements

This work is supported by the National Key R&D Program of China (Grants No. 2017YFF0209702) and funded by the National Natural Science Foundation of China (Grants No. 61527803).

References

[1] D.C. Jiles, D.L. Atherton, Theory of ferromagnetic hysteresis, J. Magnet. Magn. Mater. 61 (1–2) (1986) 48–60.
[2] A.A. Dubov, A study of metal properties using the method of magnetic memory, Metal Sci. Heat Treat. 39 (9) (1997) 401–405.
[3] H. Huang, J. Yao, Z. Li, et al., Residual magnetic field variation induced by applied magnetic field and cyclic tensile stress, NDT & E Int. 63 (2014) 38–42.
[4] J.W. Wilson, G.Y. Tian, S. Barrans, Residual magnetic field sensing for stress measurement, Sensors Actuators A: Phys. 135 (2) (2007) 381–387.
[5] M. Roskosz, Capabilities and limitations of using the residual magnetic field in NDT, in: 19th World Conference on Non-Destructive Testing, Munich Google Scholar. 2016.
[6] M. Roskosz, M.Ł. Bieniek, Evaluation of residual stress in ferromagnetic steels based on residual magnetic field measurements, NDT & E Int. 45 (1) (2012) 55–62.
[7] M. Bieniek, Analysis of the universality of the residual stress evaluation method based on residual magnetic field measurements, NDT & E Int. 54 (2013) 63–68.
[8] S. Bao, H. Lou, M. Fu, et al., Correlation of stress concentration degree with residual magnetic field of ferromagnetic steel subjected to tensile stress, Nondestr. Test. Eval. 32 (3) (2017) 255–268.
[9] S. Bao, Y. Gu, M. Fu, et al., Effect of loading speed on the stress-induced magnetic behavior of ferromagnetic steel, J. Magn. Magn. Mater. 423 (2017) 191–196.
[10] M.L. Fu, S. Bao, Z.Y. Zhao, et al., Effect of sample size on the residual magnetic field of ferromagnetic steel subjected to tensile stress, Insight-Non-Destr. Test. Cond. Monit. 60 (2) (2018) 90–94.
[11] M. Xu, M. Xu, J. Li, et al., Discuss on using Jiles-Atherton theory for charactering magnetic memory effect, J. Appl. Phys. 112 (9) (2012) 401–405.
[12] P. Shi, X. Zheng, Magnetic charge model for 3D MMM signals, Nondestr. Test. Eval. 31 (1) (2016) 45–60.
[13] A. Hubert, R. Schäfer, Magnetic Domains: The Analysis of Magnetic Microstructures, Springer Science & Business Media, 2008.
[14] J. McCord, Progress in magnetic domain observation by advanced magneto-optical microscopy, J. Phys. D: Appl. Phys. 48 (33) (2015) 333001.
[15] M.R. Koblischka, R.J. Wijngaarden, Magneto-optical investigations of superconductors, Supercond. Sci. Technol. 8 (4) (1995) 199.
[16] C. Jooss, J. Albrecht, H. Kuhn, et al., Magneto-optical studies of current distributions in high-Tc superconductors, Reports Progr. Phys. 65 (5) (2002) 651.
[17] R. Grechishkin, S. Chigirinsky, M. Gusev, et al., Magnetic imaging films, Magn. Nanostruct. Modern Technol. (2008) 195–224.
[18] W.A. Woźniak, P. Kurzynowski, M. Zdunek, Malus law – interferometric interpretation, OpticaApplicata 43 (2) (2013) 237–246.
[19] P. Shi, K. Jin, X. Zheng, A magnetomechanical model for the magnetic memory method, Int. J. Mech. Sci. 124 (2017) 229–241.
[20] z. Li, S. Dixon, P. Cawley, Study of metal magnetic memory (MMM) technique using permanently installed magnetic sensor arrays[C]//, Rev. Prog. Quan. Nondest. Eval. (2016).
[21] L. Luming, H. Songling, W. Xiaofeng, et al., Magnetic field abnormality caused by welding residual stress, J. Magn. Magn. Mater. 261 (3) (2003) 385–391.
[22] P. Mohanaiah, P. Sathyanarayana, L. GuruKumar, Image texture feature extraction using GLCM approach, Int. J. Sci. Res. Publ. 3 (5) (2013) 1.